INTEGRATED FERROELECTRICS
2021, VOL. 221, 73–87
https://doi.org/10.1080/10584587.2021.1965834

Taylor & Francis
Taylor & Francis Group

Effect and Evaluation of an Ultrasonic Atomizer With Large Vibration Amplitude

Yung Ting, Amelia Sugondo, Chih-Hsuan Yu, Yun-Jui Yang, and Yen-Lung Lee

Department of Mechanical Engineering, Chung Yuan Christian University, Chung Li-Taoyuan, Taiwan

ABSTRACT

An ultrasonic atomizer can produce large vibration amplitude is designed. Different from the structure of the usually seen ultrasonic spray nozzle, the atomizer is fundamentally constructed with a hollow tube encircled with several pieces of sectional type piezoelectric actuators, which can radially oscillate the tube to generate desired vibration profile. Atomization is formed on the surface around the liquid outlet of the tube where maximum vibration amplitude occurs. In search of resonance frequency and vibration amplitude, modal and harmonic analyses of the ultrasonic atomizer are carried out by ANSYS. In comparison the simulated results with the experimental results, both are in good agreement. A measurement system is set up for detecting the atomization droplets and calculating the droplet size and distribution. An attempt is to design an ultrasonic atomizer can produce high distribution and small diameter droplets for some application-level requirements, droplet diameter around 20–60 μm is assumed to be the specification for performance verification of the proposed atomizer. In experiment, it is found nearly 90% of atomized droplets fit for the requirement. Besides the most important factor of operating frequency, a relation of amplitude is found to include in the well-known Lang and Rayleigh's equation.

ARTICLE HISTORY
Received 8 February 2021
Accepted 15 June 2021

KEYWORDS
Ultrasonic atomization; atomizer; vibration amplitude

1. Introduction

Atomization processes have been applied in many fields, such as industry, medicine, agriculture, automotive, etc. Ultrasonic atomization is the fastest growing atomization technology at present, which has more advantages than the conventional atomization [1–7]. Ultrasonic atomization is a disintegration process of liquid sheet or ligament into small particles by using ultrasonic vibration mechanism. Capillary wave and cavitation effect are the two main reasons of liquid disintegration in the process of ultrasonic atomization [8, 9]. The former one relies on the Taylor's instability theory. The latter one usually happens in high frequency and high energy intensity systems. Through ultrasonic vibration, a combination of capillary waves on the liquid surface along with acoustic cavitation bubble oscillations beneath the liquid surface cause the droplets to be emitted. When an ultrasound wave encountering a liquid–air interface, a protuberance in the liquid surface is formed. The cavitation bubbles along with capillary waves

CONTACT Yung Ting yung@cycu.edu.tw

on the liquid surface will produce droplets in atomization. A conjunction hypothesis of ultrasonic atomization is proposed that the generated capillary wave will interact with the hydraulic shock and excite both phenomena to form droplets [10–12]. Diameter is normally measured as the size of droplet. For miscellaneous application purposes, diameter of the generated droplet for most of the existing atomizers is in a range of a few micrometers up to 500 μm [13]. A number of research works attempted to find the relation between the droplet diameter and operating conditions. Kelvin's equation described the relation among the wavelength, operating frequency, and liquid property [14]. The droplet diameter is proportional to the wavelength that was verified in experiment by Lang [15]. Further empirical studies on the influence of frequency, surface tension, density, viscosity to the droplet formation and the droplet size were carried out in various research works [1, 7–9, 16, 17]. Results and conclusions of these investigations were similar to the combination of Kelvin's and Lang's equations that the droplet size is mainly determined by the operating frequency, the surface tension, and the liquid density. Few of research articles explored the significance of vibration amplitude. For instance, studied about dependences of diameter droplet on the vibration amplitude for several frequencies and found that increasing amplitude will increase droplet diameter, increasing amplitude from 3 μm to 18 μm, the droplet diameter also increases almost linearly [5]. An atomizer was designed to observe the generated droplets with diameter of 50 μm under the condition of frequency 54 kHz and vibration amplitude 2.02 μm [9]. Different amplitudes of the two vibrating plates were employed to ascertain whether amplitude affects the droplets size [18]. However, without in-depth study, the mathematical relation between the amplitude and the droplet size was not clear.

In our previous numerical study of using Volume of Fluid (VOF) of ANSYS FLUENT 12.0, it is found that large amplitude but lower frequency is likely to make ultrasonic atomization successfully happen [19]. In this article, the proposed ultrasonic atomizer is basically constructed with a hollow tube encircled with several pieces of piezoelectric actuators that is able to gain larger vibration amplitude. The developed atomizer can demonstrate its feasibility of achieving ultrasonic atomization without driving very high frequency, which is different from a few of micro-machined ultrasonic nozzle sprays or atomizers needs to operate at frequency up to megahertz [2–4, 6, 20–24]. Moreover, an aim is to design an ultrasonic atomizer can produce high distribution and small diameter droplets for some application-level requirements, and investigate the effect of vibration amplitude on the droplet diameter. To prove the cause-and-effect thoroughly, several atomizers with the same structure but different tube length are designed to generate different vibration amplitude and produce different droplet diameter on purpose. A relation of vibration amplitude is found to include in the well-known Lang and Rayleigh's equation.

Industrial printing application is selected as an example to examine the performance of atomization. In conventional inkjet printing, the typical particle size has a resolution of 20–50 μm in diameter [25]. In printing process, such as 3D printing and speed printing, common requirement of the droplet size is around 30–60 μm in diameter [26–28]. In reference to the above applications, droplet diameter of 20–60 μm is chosen as the objective for further analysis and evaluation.

2. Ultrasonic Atomization

In ultrasonic atomization, Kelvin's and Lange's equations are probably the most well-known proof in experiment. According to Kelvin's equation, the wavelength of capillary wave is defined as [14]:

$$\lambda = \left(\frac{8\pi\sigma}{\rho f^2}\right)^{\frac{1}{3}} \tag{1}$$

where σ is surface tension; ρ is liquid density; f is ultrasonic frequency; λ is wave length. In Lang's equation, the correlation between the droplet diameter (d_p) and capillary wavelength in ultrasonic atomization process is given by [15]:

$$d_p = C\lambda \tag{2}$$

where d_p is diameter of the droplet; C is a constant found in experiment for different liquids and setting condition. As seen from (1) and (2), besides the liquid properties, frequency is another significant factor determines the droplet diameter. In our previous numerical simulation study, it is found that large amplitude is instrumental to achieve atomization [19]. The influence of vibration amplitude on the droplet diameter not included in the Kelvin's and Lang's equations is also a major focus in this article.

3. Atomizer Design

As illustrated in Figure 1, a simple structure constructed with a hollow tube encircled with piezoelectric actuators onto its outer surface is used in this study. According to our previous study of encircling different shape of piezoelectric actuators such as the ring type, 2-piece sectional type, and 3-piece sectional type around the hollow tube, it implies that the 3-piece sectional type would gain larger radial vibration effect. When tube attached with single vibration source, the wave field spray out as a sector area, it indicates the wave field will be a superimposed or destructive field occur with multi-vibration source. In previous study, the 3-piece sectional type with 90° arc length as well as 30° clearance in between the actuators would gain larger radial vibration effect [29]. The liquid outlet on the tube is assigned on the position of superposition effect as shown in Figure 2. The tube is fixed at both ends. The piezoelectric actuators are radially oscillating to vibrate the tube. Driving with appropriate frequency to match the desired vibration mode shape of the tube, expected vibration profile of the tube is

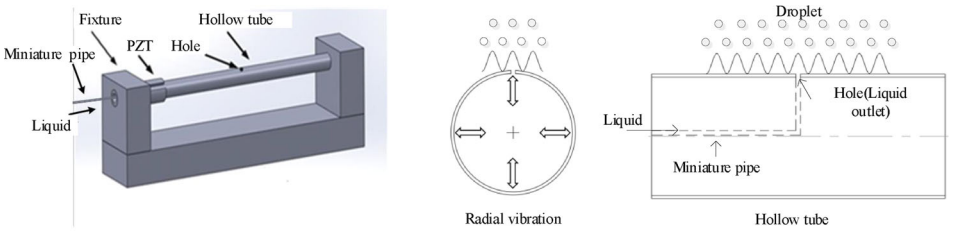

(a) Main parts of atomizer (b) Vibration on the tube & droplets around the hole

Figure 1. Structure and operating function of Atomizer.

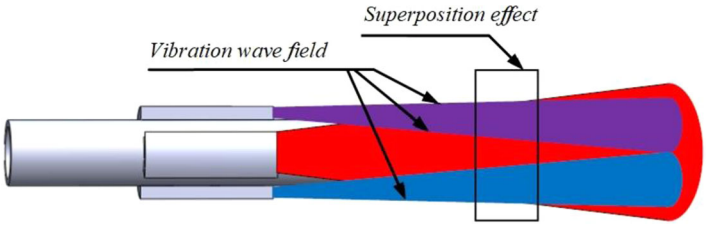

Figure 2. The superposition effect area on the tube.

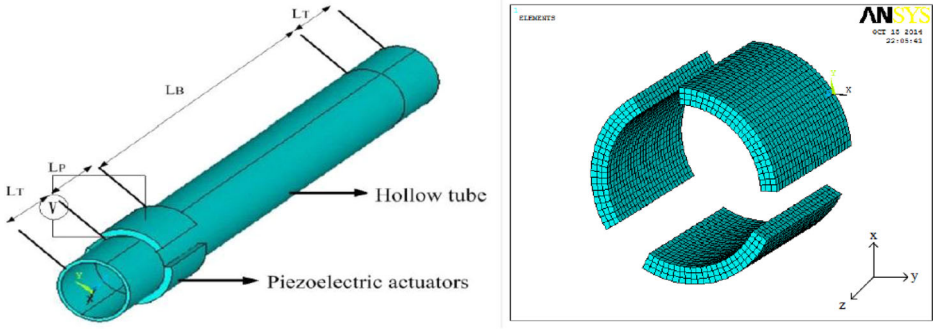

(a) Hollow tube encircled with ceramic actuators (b) Sectional-type ceramic actuators

Figure 3. Structure of hollow tube and piezoelectric actuators.

obtained. Maximum vibration amplitude would occur in certain location on the tube, which is presumed to be large enough for atomization purpose. With such fundamental structure, several atomizers with different tube length are designed to provide desired vibration mode shapes that can produce large vibration amplitude. A miniature steel pipe with inner diameter of 0.2 mm and out diameter of 0.4 mm is employed inside the hollow tube with one end in connection with a tiny hole on the tube where the maximum vibration amplitude occurs. Liquid is pressurized by a low-pressure pump to flow in the miniature pipe and then flow out through the tiny hole at very low flow rates. While encountered with ultrasonic vibration, atomization phenomenon would appear on the tube surface around the hole.

4. Modal and Harmonic Analysis

ANSYS is used for modal and harmonic analyses. Figure 3 shows a hollow tube employed with 3 pieces of sectional type of piezoelectric actuators, which have same inner diameter of 9.5 mm and outer diameter of 10.5 mm and same arc angle of 90°. Three sets of hollow tube with same inner diameter of 9 mm and outer diameter of 9.5 mm but different length L= (70,80,90)mm are used for atomizer design. L_P is the length of piezoelectric actuators. L_T represents the part of the tube embedded into the fixture. L_B is the region to generate vibration amplitude. Since the length of L_P and L_T are both assigned with constant value of 10 mm, L_B is the only variant length in the

three atomizers. Ceramics PZT-5A and steel AISI-304 is used for the piezoelectric actuator and the hollow tube, respectively.

The stiffness matrix, piezoelectric matrix, and dielectric matrix are given by

Stiffness matrix $[s]$:

$$[s] = \begin{bmatrix} 12.1 & 7.54 & 7.52 & 0 & 0 & 0 \\ 7.54 & 12.1 & 7.52 & 0 & 0 & 0 \\ 7.52 & 7.52 & 11.1 & 0 & 0 & 0 \\ 0 & 0 & 0 & 2.11 & 0 & 0 \\ 0 & 0 & 0 & 0 & 2.11 & 0 \\ 0 & 0 & 0 & 0 & 0 & 2.26 \end{bmatrix} GPa \tag{3}$$

Piezoelectric matrix $[d]$:

$$[d] = \begin{bmatrix} 0 & 0 & 0 & 0 & 12.3 & 0 \\ 0 & 0 & 0 & 12.3 & 0 & 0 \\ -5.4 & -5.4 & 15.8 & 0 & 0 & 0 \end{bmatrix} N/(V.m) \tag{4}$$

where $d31 = d32$ and $d15 = d24$.

Dielectric matrix $[\varepsilon]$:

$$[\varepsilon^T] = \begin{bmatrix} 1730 & 0 & 0 \\ 0 & 1700 & 0 \\ 0 & 0 & 1730 \end{bmatrix} \tag{5}$$

By modal analysis, desired vibration mode shape can generate large amplitude for the three atomizers is found respectively as shown in Figure 4 and listed in Table 1. By harmonic analysis, the simulated vibration amplitude is ascertained and listed in Table 2 for each case (a), (b), (c) in Figure 4 while applying input voltage Vpp from 200 V to 400 V with an increment of 25 V, respectively. As seen, for all testing cases, vibration amplitude is greater than 2.5 μm, which is expected to be enough to make atomization occur. Figures 5–7 show the examples of harmonic analysis with input voltage Vpp of 200 V and 400 V for each chosen vibration mode of Figure 3(a), (b) and (c) respectively. The exit orifice is located at 20 mm, 18.3 mm, 17.5 mm from the left end of the tube respectively, where it generates large amplitude.

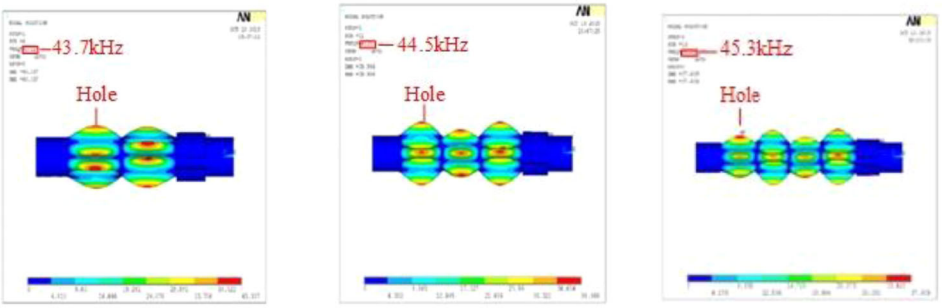

(a) L=70mm(43.7kHz) (b) L=80mm(44.5kHz) (c) L=90mm(45.3kHz)

Figure 4. Modal analysis.

Table 1. Analytical and measured resonance frequency.

Length L (mm) Methods	70	80	90
Analytical (ANSYS simulation) kHz	43.70	44.50	45.30
Measured (Impedance Analyzer) kHz	42.61	44.55	46.07
Actual (Experiment) kHz	44.10	44.90	45.50

Table 2. Analytical and measured amplitude.

Length	70 mm Amplitude μm		80 mm Amplitude μm		90 mm Amplitude μm	
Vpp	Analytic	Exp	Analytic	Exp	Analytic	Exp
200 V	3.16	3.1	5.59	3.1	3.21	3.2
225 V	3.28	3.3	3.12	3.5	3.37	3.4
250 V	3.48	3.5	3.78	3.9	3.67	3.6
275 V	3.81	3.8	4.16	4.2	4.23	4.0
300 V	4.42	4.1	4.30	4.5	4.61	4.7
325 V	4.52	4.5	5.06	5.0	5.18	5.2
350 V	5.25	4.7	5.91	5.4	6.04	5.6
375 V	5.37	5.0	5.84	5.8	6.19	6.1
400 V	6.06	5.4	6.48	6.3	6.50	6.6

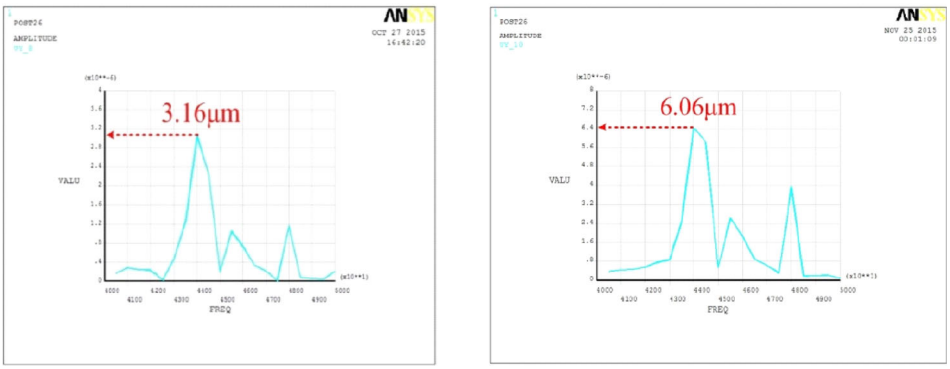

Figure 5. Amplitude – 200 V (left) and 400 V (right) @ $f = 44.1$ kHz (L = 70 mm).

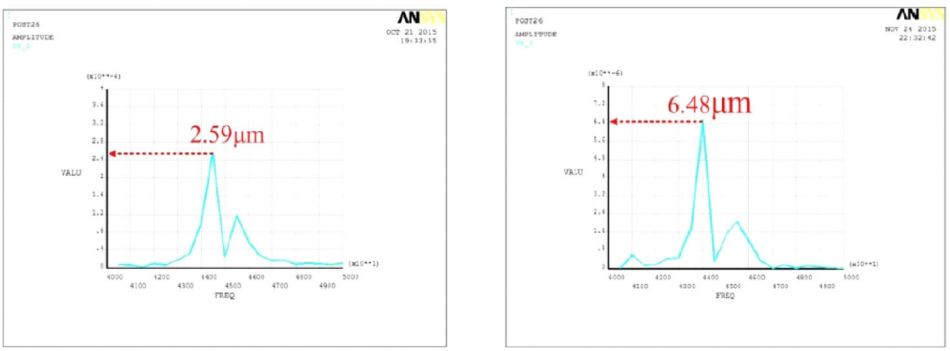

Figure 6. Amplitude – 200 V (left) and 400 V (right) @ $f = 44.9$ kHz (L = 80 mm).

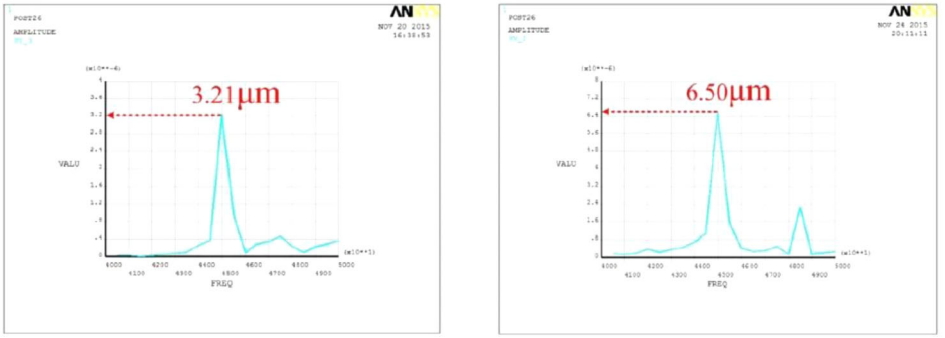

Figure 7. Amplitude – 200 V (left) and 400 V (right) @ $f = 45.5$ kHz (L = 90 mm).

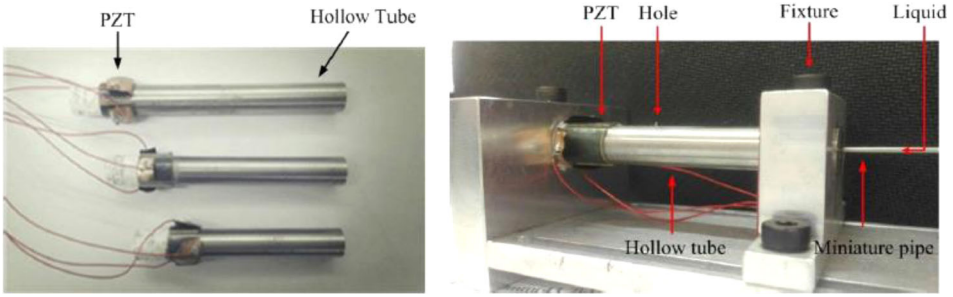

Figure 8. Photo of main parts of the atomizer.

5. Experiments

Like the above case studies in simulations, three types of tube with length L=(70,80, 90) mm encircled with 3 pieces of piezoelectric actuators are fabricated and assembled with miniature pipe etc. to form an atomizer as shown in Figure 8. The resonance frequency of each atomizer is measured by Impedance Analyzer (Agilent4294A) respectively and shown in Figure 9. The resonance frequency and anti-resonance frequency are shown at the signal curve valley and peak respectively by impedance analyzer for radial vibrator. In practice, the actual driving frequency is set to be (44.1,44.9,45.5)kHz respectively for each atomizer. As listed in Table 1, the difference among the analytical (ANSYS), measured (Impedance Analyzer), and actual frequency is very small, mainly due to mass of the fixture. The vibration amplitude is measured by a laser-Doppler vibrometer (Polytec OFV-5000 and OFV-511). While operating the actual driving frequency for each atomizer and applying the input voltage V_{pp} and the input current I_{pp} in the range of 200–400 V and 200–450 mA respectively, the generated vibration amplitude is gradually increased as shown in Figure 13. Figures 10–12 show the measured signals of the selected examples Vpp = 200 V and 400 V respectively on the oscilloscope (Agilent 33500B). The resolution of the vibrometer is 10 μm/V. For instance, in Figure 10, applying voltage of 200 V to the atomizer with length L = 70 mm, the measured vibration amplitude is calculated as 310 mV × 10 μm/V = 3.1 μm. In comparison the analytical results with the experimental results shown in Figure 13, it is seen that both are in a close approximation.

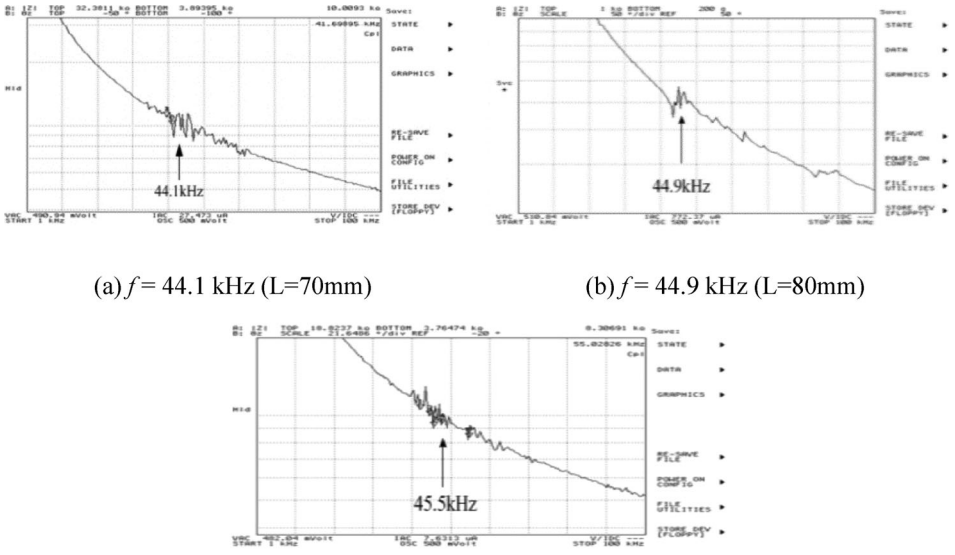

(a) f = 44.1 kHz (L=70mm) (b) f = 44.9 kHz (L=80mm)

(c) f = 45.5 kHz (L=90mm)

Figure 9. Measured resonance frequency by impedance analyzer.

(a) Applied voltage Vpp=200V (b) Applied voltage Vpp=400V

Figure 10. Measurement of vibration amplitude @44.1 kHz (L = 70 mm).

Figure 14 shows the schematic diagram of experimental setup of atomizer and measurement system. Figure 15 shows the actual experimental setup of atomizer and measurement system. A measurement system is established including high speed camera (Basler acA1300-30gm) to capture the particle image of atomization and to inspect the atomization phenomenon. A high-intensity light source is employed to assist in capturing higher quality image. Software Image J is used to analyze the particle size and the particle distribution of the image [30, 31]. The capture images were analyzed first. Then the "in-focus" droplet images which the droplet images are sharp compared to the dark background were chosen. By introducing multiple intensity levels, the droplet is defined with a "halo" of $\Delta d/2$, where d yields the actual diameter of the droplet around the droplets. The out-of-focus droplets were determined and eliminated by fixing the

(a) Applied voltage Vpp=200V (b) Applied voltage Vpp=400V

Figure 11. Measurement of vibration amplitude @44.9 kHz (L = 80 mm).

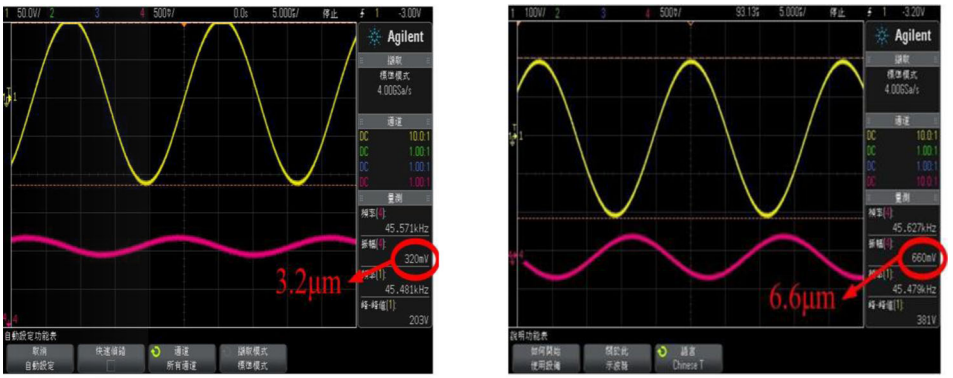

(a) Applied voltage Vpp=200V (b) Applied voltage Vpp=400V

Figure 12. Measurement of vibration amplitude @45.5 kHz (L = 90 mm).

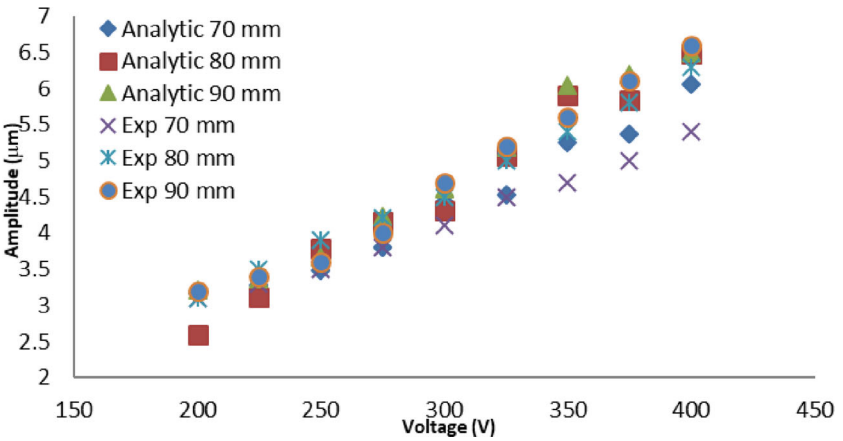

Figure 13. Analytical and measured amplitude.

intensity level. In shape analysis, the shape factor defined by perimeter^2/area is calculated. If the shape factor is greater than 4π, the droplet is determined as noncircular droplets and eliminated [32]. The calculation of droplet size is based on the equivalent

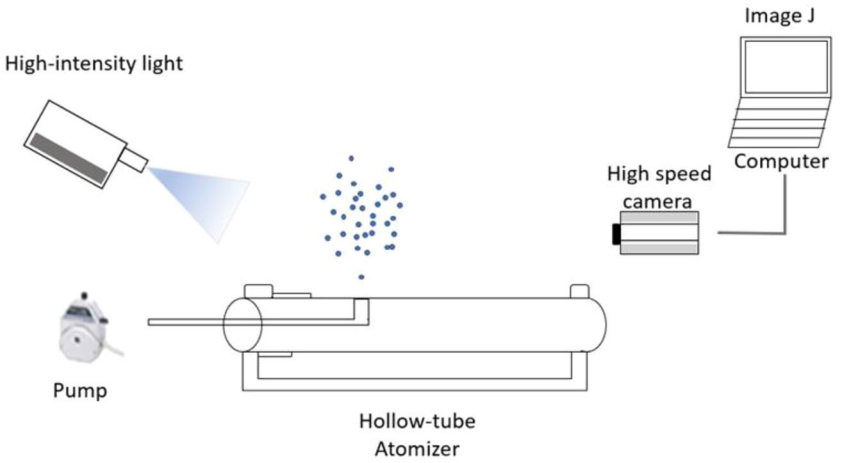

Figure 14. The schematic diagram of experimental setup and measurement system.

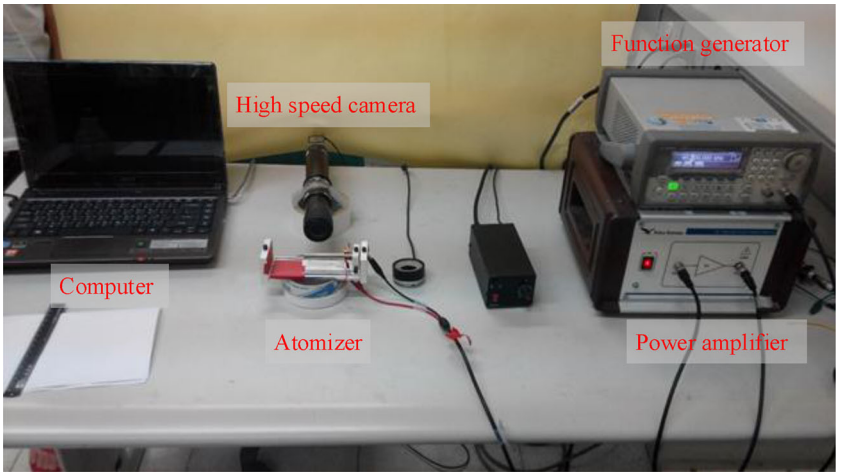

Figure 15. Experimental setup of atomizer and measurement system.

diameter defined as $D_p = 2\sqrt{A_p/\pi}$, where D_p is the equivalent diameter and A_p is the area of the droplet [33]. By eliminating both the out-of-focus and noncircular droplets, the droplets size and mean value can be calculated. In this study, each of the different vibration amplitude was repeated 5 times in experiment. And, at least 10 images were captured and analyzed. The measured droplet size was in the range of 10–70 μm, about a total 5000 droplets were detected. The dominant diameter size, for example, is about 40 μm and 30 μm by vibration amplitude of 6.6 μm and 2.5 μm respectively. In this study, water with density 998.2 kg/m^3, viscosity 0.001003 kg/m-s, and surface tension 0.0728 N/m is selected as an example for atomization. As a result, atomization is successfully achieved with large enough vibration amplitude in the range of 3.1–6.6 μm. Figure 16 shows the captured image of atomization for different vibration amplitude and frequency. Figure 17 shows the trend of droplet diameter versus vibration amplitude. As seen, while increasing vibration amplitude can obtain larger droplet diameter. While applied 400 V_{pp}, the size and distribution are 7% under 20 μm, 4% greater than

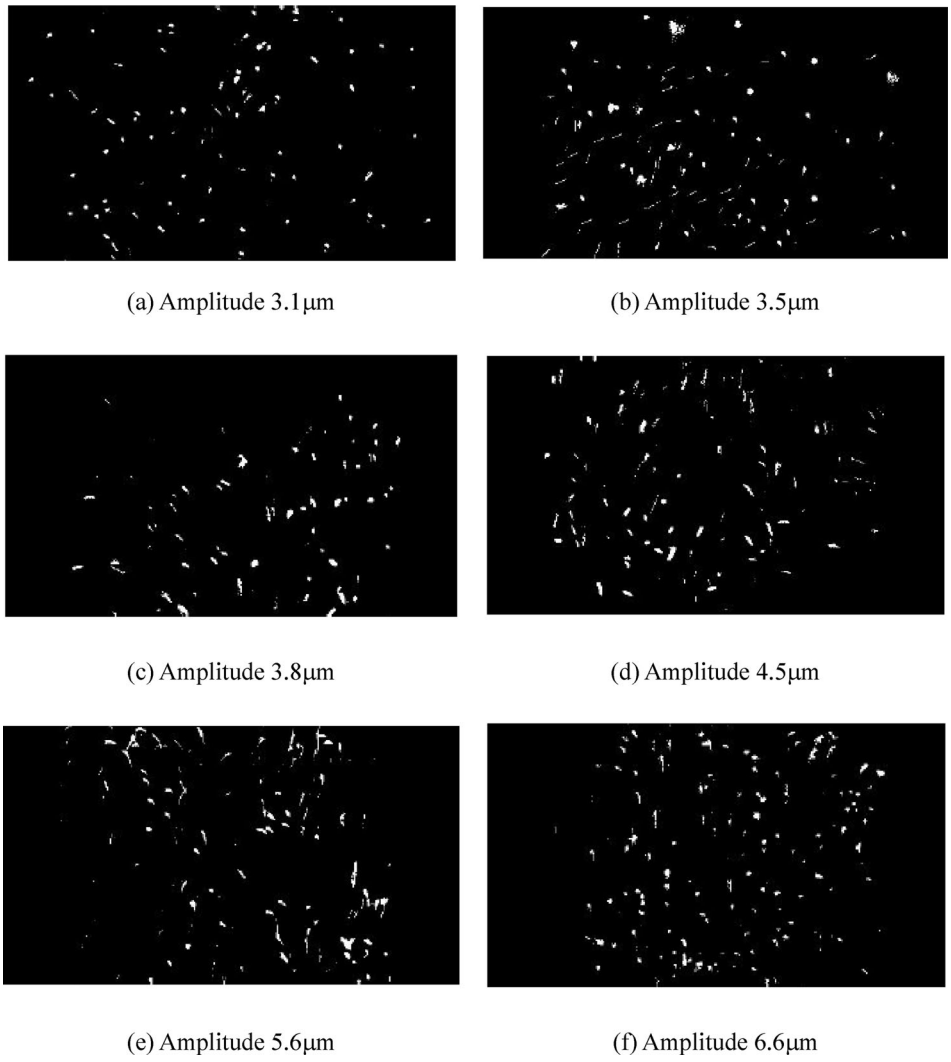

Figure 16. Captured image of atomized particle.

60 μm, thus 89% fits for the application example of industrial printing specification. Moreover, there are 86% in the range of 20–50 μm and 77% in the range of 20–40 μm. A nearly linear relationship appears between the amplitude and the droplet diameter in this study. This interesting phenomenon implies that large vibration amplitude at adequate frequency can make atomization happen but will engender large droplet diameter. Droplet particles are not generated when applied vibration amplitude is not enough to generate capillary wave. Such fact is reasonable because large amplitude is instrumental to aggravate cavitation effect and produce larger size of droplet.

According to the above correlation of the droplet size and the vibration amplitude, it implies that amplitude is also a crucial factor in droplet diameter. In other words, the vibration amplitude is instrumental to energize the liquid film to generate droplet particle. Considering a proportional relationship between the droplet diameter and the

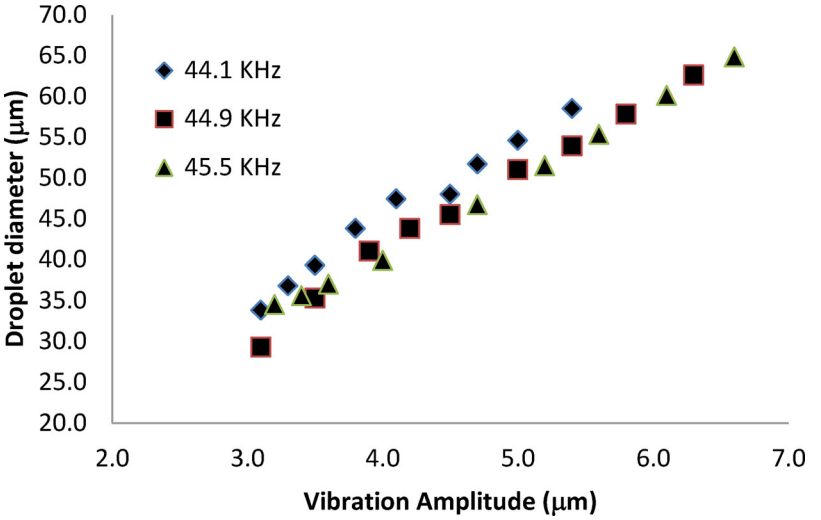

Figure 17. Droplet diameter vs. amplitude at different frequency.

vibration amplitude, an attempt is to include this effect into the Kelvin's and Lang's equations in (1) and (2) as below.

$$d_p = c\left(\frac{8\pi\sigma}{\rho f^2}\right)^{\frac{1}{3}} A^n \tag{6}$$

where n is the order of amplitude needs to be searched.

Concerning with same liquid properties, the influence on the droplet diameter due to frequency and vibration amplitude can be separate for further discussion. That is, the above (6) is rewritten as:

$$\frac{d_p}{\left(\frac{8\pi\sigma}{\rho f^2}\right)^{\frac{1}{3}}} = cA^n \tag{7}$$

Assuming the left-hand side of (7) is known in experiment and defined by y, it can be formulated by $y = \mathrm{c.A}^n$. To solve the number n, it is rewritten as:

$$\log y = \log c + n \log A \tag{8}$$

By using a linear regression function in MS Excel tool, the intercept and the coefficient n are found as show in Figure 18 that shows the relation between log A and log y of equation (8) with R-squared near to one. Its show how close the data fit to the regression line. The intercept is shows as log c = −0.914, hence $c = 0.122$. The coefficient n is found 0.914, which is approximate to one. Therefore, (6) can be written as:

$$d_p = 0.122\left(\frac{8\pi\sigma}{\rho f^2}\right)^{\frac{1}{3}} A^{0.914} \tag{9}$$

From (9) show that correlation between droplet diameter and amplitude, which means the droplet diameter is approximately proportional to the vibration amplitude at certain frequency.

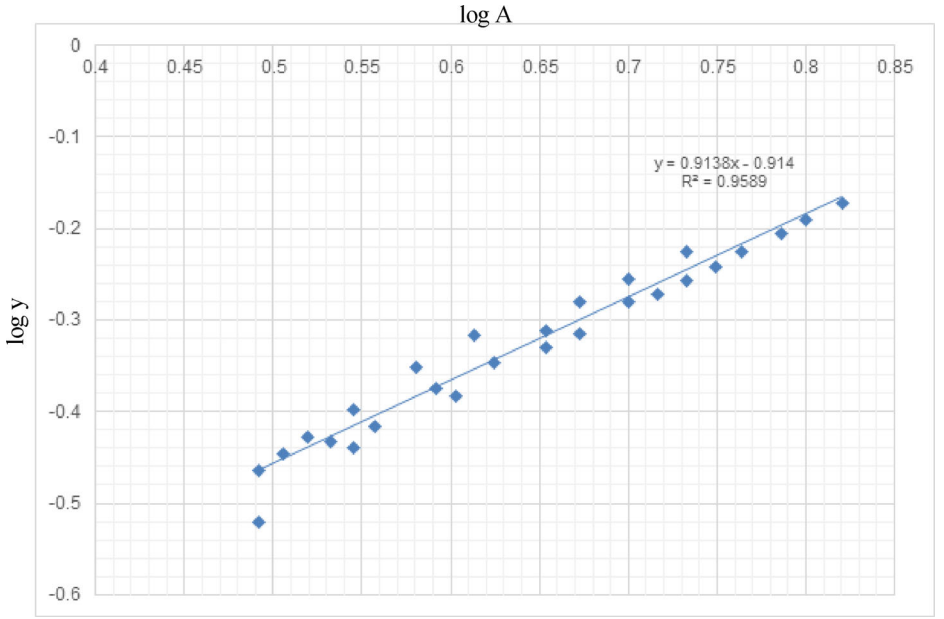

Figure 18. Relation of the two quantities in (8).

6. Conclusion

A new type of atomizer constructed with a hollow tube and 3-piece piezoelectric actuators is designed for the purpose of generating large amplitude under low frequency. In this study, for example, driving frequency around 44–46 kHz and vibration amplitude greater than 3.1 μm will be enough to make atomization occur. Nearly 90% of the atomized droplets with diameter in the range of 20–60 μm suitable for industrial printing applications is obtained. The higher vibration amplitude is employed the larger size of droplet is gained. Moreover, influence of vibration amplitude is likely included in the combined Kelvin's and Lang's equations to derive a formula as expressed by (6). The order n in (6) is equal to approximately one, which means the droplet diameter is approximately proportional to the vibration amplitude at certain frequency. To sum up, without operating very high frequency of mega-hertz, the proposed atomizer is able to achieve atomization and produce acceptable droplet size. The maximum driving current I_{max} is approximate to $I_{max} \approx f \times C_p \times V_{pp} \times \pi$ where C_p is the equivalent capacitor of piezoelectric ceramic. Assuming the driving voltage for most of the atomizer is in the range of 200–400 Vpp in general, the actual driving power is proportionally reduced while the frequency is reduced from several Megahertz to around 40 kHz. The atomization system driving circuitry and is therefore simplified as well as cost-effective due to reduction of driving power. This advantage encourages the development of similar type of ultrasonic transducer providing large enough amplitude but operating at lower ultrasonic frequency. Regarding a linear relation between the vibration amplitude and the droplet diameter, liquid flowrate, atomization rate versus applied voltage, exit velocity of the atomized droplets, etc., it needs more examinations with various types of liquids and operating conditions to verify the fact, which will be tackled in the near future.

Acknowledgment

Thanks Professor Huei Chu Weng for his instruction on fluid dynamics.

Funding

This research was sponsored NSC98-2221-E-033-015 by Soundwide Technology Corp.

References

1. M. Dobre, and L. Bolle, Visualisation and analysis of liquid film surface patterns formed on ultrasonic atomisers, ILASS, Toulouse, France (1999).
2. K. S. Hedrih, V. Babović, and D. Šarković, An auxiliary size distribution model for the ultrasonically produced water droplets, *Exp. Therm. Fluid Sci.* **30** (6), 559 (2006). DOI: 10.1016/j.expthermflusci.2005.12.001.
3. Y.-L. Huang, and S.-H. Chang, Micro-droplets atomizer using PZT ring actuator, *J. Mech.* **26** (3), 423 (2010). DOI: 10.1017/S1727719100003981.
4. T. Harada *et al.*, Droplet generation using a torsional Langevin-type transducer and a micropore plate, *Sens. Actuators, A.* **155** (1), 168 (2009). DOI: 10.1016/j.sna.2009.08.007.
5. V. Khmelev *et al.*, Determination of the modes and the conditions of ultrasonic spraying providing specified productivity and dispersed characteristics of the aerosol, *JAFM* **10** (5), 1409 (2017). DOI: 10.18869/acadpub.jafm.73.242.26620.
6. M. Tembely, C. Lecot, and A. Soucemarianadin, Prediction and evolution of drop-size distribution for a new ultrasonic atomizer, *Appl. Therm. Eng.* **31** (5), 656 (2011). DOI: 10.1016/j.applthermaleng.2010.09.027.
7. K. A. Ramisetty, A. B. Pandit, and P. R. Gogate, Investigations into ultrasound induced atomization, *Ultrason. Sonochem.* **20** (1), 254 (2013). DOI: 10.1016/j.ultsonch.2012.05.001.
8. B. Avvaru *et al.*, Ultrasonic atomization: Effect of liquid phase properties, *Ultrasonics* **44** (2), 146 (2006). DOI: 10.1016/j.ultras.2005.09.003.
9. R. Rajan, and A. B. Pandit, Correlations to predict droplet size in ultrasonic atomisation, *Ultrasonics* **39** (4), 235 (2001). DOI: 10.1016/S0041-624X(01)00054-3.
10. Y. Boguslavski, Physical mechanism of the acoustic atomization of a liquid, *Sov. Phys. Acoust.* **15**, 14 (1969).
11. D. Briceño-Gutierrez *et al.*, On the ultrasonic atomization of liquids, *Phys. Proc.* **63**, 37 (2015). DOI: 10.1016/j.phpro.2015.03.006.
12. J. C. Simon *et al.*, Ultrasonic atomization of liquids in drop-chain acoustic fountains, *J. Fluid Mech.* **766**, 129 (2015). DOI: 10.1017/jfm.2015.11.
13. A. H. Lefebvre, *Atomization and Sprays* (Hemisphere Pub, Corp., New York, NY, 1989).
14. J. W. S. B. Rayleigh, *The Theory of Sound* (Macmillan, Basingstoke, UK, 1896).
15. R. J. Lang, Ultrasonic atomization of liquids, *J. Acoust. Soc. Am.* **34** (1), 6 (1962). DOI: 10.1121/1.1909020.
16. M. Dobre, and L. Bolle, Practical design of ultrasonic spray devices: Experimental testing of several atomizer geometries, *Exp. Therm. Fluid Sci.* **26** (2-4), 205 (2002). DOI: 10.1016/S0894-1777(02)00128-0.
17. K. Yasuda *et al.*, Ultrasonic atomization amount for different frequencies, *Jpn. J. Appl. Phys.* **50** (7S), 07HE23 (2011). DOI: 10.7567/JJAP.50.07HE23.
18. T. Asami *et al.*, Ultrasonic atomization by difference between vibration displacements of two circular vibrating plates, *J. Mech. Eng. Automat.* **2** (6), 30 (2016).
19. C.-H. Yu, A. Sugondo, and Y. Ting, Numerical simulation and performance evaluation of droplet particle formation by using a new approach of ultrasonic atomization, in IEEE International Ultrasonics Symposium, Chicago, IL, 2014.
20. A. Lal, and R. M. White, Micromachined silicon ultrasonic atomizer, in 1996 IEEE Ultrasonics Symposium. Proceedings, vol. 1, IEEE, 1996, pp. 339–342.

21. E.-S. R. Negeed *et al.*, Experimental and analytical investigation of liquid sheet breakup characteristics, *Int. J. Heat Fluid Flow* **32** (1), 95 (2011). DOI: 10.1016/j.ijheatfluidflow.2010.08.005.
22. R. R. Perron, The design and application of a reliable ultrasonic atomizer, *IEEE Trans. Son. Ultrason.* **14** (4), 149 (1967). DOI: 10.1109/T-SU.1967.29430.
23. S. C. Tsai *et al.*, Silicon-based megahertz ultrasonic nozzles for production of monodisperse micrometer-sized droplets, *IEEE Trans. Ultrason. Ferroelectr. Freq. Control* **56** (9), 1968 (2009). DOI: 10.1109/TUFFC.2009.1273.
24. N. Maehara, S. Ueha, and E. Mori, Optimum design procedure for multi-pinhole-plate ultrasonic atomizer, *Jpn. J. Appl. Phys.* **26** (S1), 215 (1987). DOI: 10.7567/JJAPS.26S1.215.
25. Z. Cui, *Printed Electronics: Materials, Technologies and Applications* (John Wiley & Sons, Hoboken, NJ, 2016).
26. Arthur Cassaihnau, 2015, Understanding our 60 mm layer thickness printing setting, Sculptro (accessed Sep 2021), https://www.sculpteo.com/blog/2015/04/30/60%C2%B5m-layer-thickness-3d-printing.
27. MiiCraft, MiiCraft 125 series Tech Specs. MiiCraft (accessed Sep 2021), https://miicraft.com/product/miicraft-125-series-tech-specs.
28. BIOFORCE NANOSCIENCES, Application note 203 – "speed printing"; or, printing in "no laser mode" with the nano enabler system™. BIOFORCE NANOSCIENCES (accessed Sep 2021), http://bioforcenano.com/resources/aapplication-note-203-speed-printing-or-printing-in-no-laser-mode-with-the-nano-enabler-system.
29. T.-S. Tsai, Design and application of hollow cylindrical piezoelectric vibrator. Master thesis, Mechanical Engineering, Chung Yuan Christian University, 2012.
30. C. A. Sennoga, E. Kanbar, and A. Bouakaz, An ImageJ plugin for the sizing and counting of microbubbles, in 2015 IEEE International Ultrasonics Symposium (IUS), IEEE, 2015, pp. 1–4. DOI: 10.1109/ULTSYM.2015.0483.
31. R. Lind, Open source software for image processing and analysis: Picture this with ImageJ in *Open Source Software in Life Science Research* (Elsevier, New York, NY, 2012), pp. 131–149.
32. E. Fantini, L. Tognotti, and A. Tonazzini, Drop size distribution in sprays by image processing, *Comput. Chem. Eng.* **14** (11), 1201 (1990). DOI: 10.1016/0098-1354(90)80002-S.
33. N. Lad, A. Aroussi, and M. M. Sa, Droplet size measurement for liquid spray using digital image analysis technique, *J. Appl. Sci.* **11** (11), 1966 (2011). DOI: 10.3923/jas.2011.1966.1972.